Landau theory of the magnetic phase diagram of monoclinic multiferroics: Application to $MnWO_4$ and CuO

G. Quirion and M. L. Plumer

Department of Physics and Physical Oceanography, Memorial University, St. John's, Newfoundland, Canada, A1B 3X7

(Received 30 March 2013; revised manuscript received 10 May 2013; published 24 May 2013)

We present a detailed analysis of the magnetic states of monoclinic multiferroic systems as a function of temperature and magnetic field. The proposed nonlocal Landau free energy derived using symmetry arguments accounts well for the phase diagram of $MnWO_4$ with the field applied along each of the three principal crystallographic directions. A description is proposed for the high field magnetic spin configurations, above 10 T, which have not yet been identified by neutron scattering. The nature of the induced electric polarization in each of the magnetic states is described. Corresponding results for CuO are also presented.

DOI: 10.1103/PhysRevB.87.174428 PACS number(s): 75.85.+t, 75.10.Hk, 75.30.Kz, 75.50.Ee

I. INTRODUCTION

A common feature of a large number of multiferroics is ferroelectricity induced by a spiral magnetic order associated with magnetic frustration.[1,2] Noncollinear magnetic order breaks the inversion symmetry giving rise to magnetoelectric coupling and the coexistence of magnetic and ferroelectric order.[3,4] In some cases this can occur at high temperatures and therefore this class of magnetically frustrated multiferroics offers new opportunities for technological applications.[5]

The interest in this field has grown considerably after the discovery of new materials such as rare-earth (R) manganites $RMnO_3$, RMn_2O_5,[1,6] geometrically frustrated systems $CuMO_2$ (M is Fe or Cr),[7,8] and monoclinic multiferroic compounds like CuO and $MnWO_4$.[9–11] Even though these materials can belong to a different point group in the paramagnetic state, the magnetoelectric effect is regularly observed in the monoclinic structural phase, which is the case for $CuMO_2$, CuO, and $MnWO_4$. Elucidating the nature of the often complex spin structures can serve to further our understanding of how ferroelectric and magnetic order are linked in monoclinic systems and multiferroics in general. Among all these materials, $MnWO_4$ has been the subject of many experimental and theoretical studies.[11–18] In particular, the magnetic phase diagram of $MnWO_4$ has been determined up to 60 T with the field applied along the three principal crystallographic directions.[19] Up to seven magnetic states have been determined. Moreover, polarization measurements have identified three states for which the magnetic and ferroelectric order coexist. Thus, this extensive set of experimental data offers a unique opportunity to test theoretical models for monoclinic multiferroics in general.

Encouraged by our recent successes on modeling the magnetic phase diagram of CuO,[20] we extend here this development of a nonlocal Landau-type free energy to study a wider class of monoclinic multiferroics. This phenomenological model, which takes into consideration the crystalline anisotropy and the magnetoelectric coupling, successfully accounts for the magnetic phase diagrams of $MnWO_4$ for different field directions. The model is also used to identify the high-field spin configuration of magnetic orders not yet determined by neutron scattering measurements. Features of the spiral orders leading to a ferroelectric polarization are also determined and an application of the model is made to CuO.

In Sec. II we provide a short description of the symmetry, structural, magnetic properties, and ferroelectric properties of $MnWO_4$ relevant to the model. In Sec. III, details regarding the derivation of the Landau free energy and the magnetoelectric coupling are given. The magnetic phase diagrams, for different field directions, are presented in Sec. IV using a set of numerical parameters determined using the main characteristics of $MnWO_4$. The nature of the spin configurations associated with the different magnetic orders, as well as results regarding the electric polarization, are presented in Secs. IV A–IV D. In Sec.V we present the magnetic phase diagram of CuO using the same model. Finally, the principal results are summarized and discussed in Sec. VI.

II. PROPERTIES OF $MnWO_4$

Like other magnetoelectric compounds ($CuFeO_2$, $CuCrO_2$, and CuO), the low temperature point group of $MnWO_4$ is monoclinic (space group $P2/c$). Furthermore, this particular multiferroic can be viewed as zigzag chains along the c axis (see Ref. 14) with two Mn^{2+} magnetic ions per unit cell ($S = 5/2$), located at $\tau_1 = (0.5, y, 0.25)$ and $\tau_2 = (0.5, 1 - y, 0.75)$ with $y = 0.685$.[12] According to neutron scattering experiments the magnetization easy axis, in the ac plane, is at an angle of 37° from the monoclinic a axis, while the twofold symmetry axis is along the b axis. As with CuO,[20] $MnWO_4$ exhibits three antiferromagnetic phases (AF1, AF2, and AF3) at zero field. The low temperature phase AF1 ($T_{N1} = 7.4$ K) corresponds to a commensurate collinear $\uparrow\uparrow\downarrow\downarrow$ spin order with wave vector $(-1/4, 1/2, 1/2)$ and the moments pointing along the easy axis. The intermediate phase AF2 ($T_{N2} = 12.5$ K) is a spiral state with moments in a plane defined by the easy axis and the b axis. Finally, the high temperature phase AF3 ($T_{N3} = 13.5$ K) is associated with an incommensurate sinusoidal modulation with moments only ordered along the easy axis. Both incommensurate phases share the same wave vector $(-0.214, 1/2, 0.457)$.

Recently, sound velocity[15] and electric polarization[19] measurements have been used to extend the magnetic phase diagram of $MnWO_4$ up to 60 T. According to these results, three additional phases are detected (HF, IV, and V) with the magnetic field parallel to the easy axis, while two new phases (X and V′) are induced with the field along the b axis. It has also been shown that phase IV sustains a ferroelectric polarization

along the b axis (as in AF2), while the polarization switches to be along the a axis in phase X.[10,19] Considering that polarized neutron diffraction measurements in $MnWO_4$[11,21] show a clear correlation between the induced ferroelectric polarization and the AF2 chiral magnetic order, these recent results suggest that the new phases IV and X might be associated with a chiral magnetic order. Since no neutron scattering data exist above 10 T, the exact spin configuration of the field induced magnetic orders remain unknown. Analysis of the proposed nonlocal Landau-type free energy helps to elucidate the nature of the AFM states observed in $MnWO_4$ and possibly in other monoclinic multiferroics.

III. THE MODEL

The derivation presented here is essentially based on the formulation of a nonlocal Landau free-energy which is known to successfully accounts for the phase diagram and properties of triangular antiferromagnets[22–25] as well as some multiferroics ($CuFeO_2$ and CuO).[20,26] As in previous contributions, the integral form of the free energy F_s is represented by a Taylor expansion in terms of the spin density $\mathbf{s}(\mathbf{r})$:

$$F_s = \frac{1}{2V}\int d\mathbf{r_1}d\mathbf{r_2}A_{ij}(\mathbf{r_1}-\mathbf{r_2})s_i(\mathbf{r_1})s_j(\mathbf{r_2}) + \frac{1}{4V}\int d\mathbf{r_1}d\mathbf{r_2}d\mathbf{r_3}d\mathbf{r_4}B_{ijkl}(\mathbf{r_1},\mathbf{r_2};\mathbf{r_3},\mathbf{r_4})s_i(\mathbf{r_1}) \times s_j(\mathbf{r_2})s_k(\mathbf{r_3})s_l(\mathbf{r_4}) - \int \mathbf{s}(\mathbf{r})\cdot\mathbf{H}d\mathbf{r}, \quad (1)$$

where repeated indices represent summations relative to the coordinates $i,j,k,l = a,b,c'$. For convenience we define the spin density using a cartesian coordinate system such that $a \perp b \perp c'$, where a and b coincide with the monoclinic crystal axes (the twofold monoclinic symmetry axis being the b direction), while $\mathbf{c}'$ is almost parallel to $\mathbf{c}$. For simplification, the expansion is truncated to four-order terms with the addition of a Zeeman energy term [last term of Eq. (1)]. All independent contributions to F are then evaluated using a magnetic moment density $\mathbf{s}(\mathbf{r})$ defined in term of a spin density $\rho(\mathbf{r})$ such that

$$\mathbf{s}(\mathbf{r}) = \frac{V}{N}\sum_R \rho(\mathbf{r})\delta(\mathbf{r}-\mathbf{R}), \quad (2)$$

with $\mathbf{R}$ representing the lattice coordinates of the magnetic Mn^{2+} ions ($S = 5/2$). In conformity with experimental observations[12] we assume that the spin density is modulated by a single wave vector $\mathbf{Q}$ describing the long-range magnetic order such that

$$\rho(\mathbf{r}) = \mathbf{m} + \mathbf{S}e^{i\mathbf{Q}\cdot\mathbf{r}} + \mathbf{S}^*e^{-i\mathbf{Q}\cdot\mathbf{r}}, \quad (3)$$

where $\mathbf{S}$ is the spin polarization vector and $\mathbf{m}$ is the induced magnetization.

The free energy must be invariant with respect to the point group operations of the corresponding space group $P2/c$. This includes a twofold symmetry operation along the b axis from which we identify four second order invariants (A_{ij}). These contributions are written in terms of the usual temperature dependent isotropic term $A_Q\mathbf{S}\cdot\mathbf{S}^* = a(T+T_Q)\mathbf{S}\cdot\mathbf{S}^*$ and three anisotropic terms. In order to focus on the most relevant terms, only anisotropy terms in $\mathbf{S}$ at second order are included. In the absence of a first-principles calculation, such as from density functional theory, it is difficult to estimate the relative magnitudes of these three phenomenological coefficients. After integrating over the spatial degrees of freedom, the free energy can be expressed as

$$F_s = A_Q\mathbf{S}\cdot\mathbf{S}^* + A_{aa}S_aS_a^* + A_{bb}S_bS_b^* + \frac{A_{ac'}}{2}(S_aS_{c'}^* + S_a^*S_{c'}) + B_1(\mathbf{S}\cdot\mathbf{S}^*)^2 + \frac{B_2}{2}|\mathbf{S}\cdot\mathbf{S}|^2 + \frac{B_u}{4}[(\mathbf{S}\cdot\mathbf{S})^2 + (\mathbf{S}^*\cdot\mathbf{S}^*)^2]\Delta_{4Q,G} + \frac{1}{2}A_om^2 + \frac{1}{4}B_3m^4 + 2B_4|\mathbf{m}\cdot\mathbf{S}|^2 + B_5m^2\mathbf{S}\cdot\mathbf{S}^* - \mathbf{m}\cdot\mathbf{H}, \quad (4)$$

where $A_o = a(T-T_o)$. Note that the lattice periodicity allows for an umklapp term $\Delta_{4Q,G}$. This particular term leads to first order transitions and accounts for the period-4 commensurate states observed at low temperatures in CuO, $CuFeO_2$, and $MnWO_4$.[7,9,12] In order to account for noncollinear magnetic configurations the complex spin polarization vector is expressed in the general form

$$\mathbf{S} = \mathbf{S_1} + i\mathbf{S_2}. \quad (5)$$

In our previous applications of the Landau free energy, an analysis of the exchange interactions through $J(\mathbf{Q})$ was included in order to account for the incommensurate wave vector $\mathbf{Q}$ and the relation $T_Q = J(Q)/a$.[20,26] For the case of $MnWO_4$ we refer the readers to the thorough discussion given by Matityahu *et al.*[17] This approach, based on quadratic exchange terms, leads to a temperature or magnetic field independent Q value (only a small effect has been observed in $Mn_{1-x}Co_xWO_4$).[27] Higher order biquadratic exchange coupling terms that can arise from spin-lattice interactions give models which yield such temperature or field dependence.[28] Dependency of the orientation of the wave vector relative to the spin polarization vector might also be accounted for through the addition of anisotropic exchange interactions as well as the magnetoelectric coupling term discussed below. These secondary effects are not included in the present work as our main focus is on a description of the spin configurations in the magnetic phase diagram.

The present study also omits the effects of higher harmonics in Q on the Fourier expansion of the spin density [Eq. (3)]. These can lead to slight distortions of the spin configuration (which have not been reported for $MnWO_4$) as well as contributions to the free energy at sixth order in $\mathbf{s}$.[29,30] The inclusion of these and other higher-order contributions to the free energy would modify the quantitative results presented below but are not required to explain the phase diagram.

To account for the electric polarization, due to chiral states, terms associated with the induced polarization $\mathbf{P}$ due to the magnetoelectric coupling are included in the free energy F_E. For magnetoelectric monoclinic systems this gives low-order contributions

$$F_E = \frac{1}{2}\frac{P_a^2}{\chi_a} + \frac{1}{2}\frac{P_b^2}{\chi_b} + \frac{1}{2}\frac{P_{c'}^2}{\chi_{c'}} + F_{\mathrm{ME}}, \quad (6)$$

where χ_i ($i = a,b,c'$) represents the dielectric susceptibility of the paraelectric phase along the principal axes ($\chi_{c'} \sim \chi_c$).

For the present analysis, it is assumed that magnetoelectric coupling energy $F_{\rm ME}$ is due to the inverse Dzyaloshinskii-Moriya (DM) or the spin-current model[31,32] as they account for the experimental results in this class of systems. The magnetoelectric energy can be then expressed as

$$\mathbf{F}_{\rm ME} = \left\{ \frac{1}{2V} \int d\mathbf{r_1} d\mathbf{r_2} \alpha(\boldsymbol{\tau}) \boldsymbol{\tau} \times [\mathbf{s}(\mathbf{r_1}) \times \mathbf{s}(\mathbf{r_2})] \right\} \cdot \mathbf{P}$$
$$= -\frac{2}{N} \sum_{\tau} \alpha(\boldsymbol{\tau}) \sin(\mathbf{Q} \cdot \boldsymbol{\tau}) (\hat{\boldsymbol{\tau}} \times [\mathbf{S}_1 \times \mathbf{S}_2]) \cdot \mathbf{P}, \qquad (7)$$

which depends on the double cross product between the spin density $\mathbf{s}(\mathbf{r_1})$, $\mathbf{s}(\mathbf{r_2})$, and the vector $\boldsymbol{\tau} = \mathbf{r}_1 - \mathbf{r}_2$ connecting both moments, with $\alpha(\boldsymbol{\tau})$ being a coupling coefficient. For a spin modulation with a wave vector $\mathbf{Q}$, the magnetoelectric energy can be more conveniently written as a function of the spin polarization vectors $\mathbf{S}_1$ and $\mathbf{S}_2$ as above.

Considering that $MnWO_4$ can be treated as a set of zigzag chain parallel to the c axis, with magnetic nearest neighbors located at $\boldsymbol{\tau}_1 = (0.5, y, 0.25)$ and $\boldsymbol{\tau}_2 = (0.5, 1-y, 0.75)$ with $y = 0.685$,[12] the magnetoelectric energy (with $\mathbf{Q}$ taken to be the commensurate value for convenience) reduced to

$$\mathbf{F}_{\rm ME} = -\alpha \sin(2\pi y)[(S_{1a}S_{2c'} - S_{1c'}S_{2a})P_a$$
$$+ (S_{1b}S_{2c'} - S_{1c'}S_{2b})P_b]. \qquad (8)$$

This result immediate indicates that the mechanism considered here can account for a spin-driven electric polarization pointing in the ab plane, consistent with the experimental observations.[19] Also note that this result shows that the zigzag structure of the chains ($y \neq 0$) plays a crucial role in the existence of an electric polarization in $MnWO_4$.

IV. MAGNETIC PHASE DIAGRAM OF $MnWO_4$

A number of Landau-type models have been proposed to account for the magnetic properties of $MnWO_4$.[16–18] However, in general these consider only one or two of the anisotropic contributions. As shown below, all of the allowed second-order anisotropic terms (A_{ij}) play a crucial role in the determination of the spin states and phase diagrams of $MnWO_4$. Here the relative values of these coefficients are set using a few key experimental results. Considering that the easy axis is in the ac plane, with a secondary easy axis along b (determined by neutron scattering),[12] we impose that $|A_{ac'}| > |A_{bb}| > |A_{aa}|$. Moreover, minimization of Eq. (1) indicates that the direction of the easy axis ($\gamma = 37^\circ$) is given by $\tan(2\gamma) = A_{ac'}/A_{aa}$. Thus, in order to reproduce the phase sequence for $0 < T < 1.2$, we set $a = 1$, $T_Q = 1.18$, $T_o = -1.0$, $A_{ac'} = -0.03$, $A_{bb} = -0.0115$, and $A_{aa} = -0.011$. All other coefficients are determined using analytical and numerical results associated with a set of conveniently defined critical values such that $T_{N3} = 1.2$, $T_{N2} = 1.11$, $H_c(T = 1.15) = 1.35$, and a maximum critical field $H_c(T = 0) = 6.0$. Therefore, $B_1 = 0.103$, $B_2 = 0.011$, $B_3 = 0.0633$, $B_4 = 0.0125$, while we set $B_5 = 0.1$ for convenience. Considering that the low temperature phase (AF1) is attributed to the period-4 umklapp term, the coefficients $B_u = 0.0206$ and $T_{(Q=G/4)} = 1.15$ have been used to reproduce a first order phase transition at $T_{N1} = 0.19$. Finally, the numerical values used for the dielectric susceptibility have been set based on experimental results[10] such that $\chi_a = 15.3$, $\chi_b = 12.2$, and $\chi'_c = 11.0$, with a magnetoelectric coupling coefficient arbitrary set to $\zeta = 0.015$.

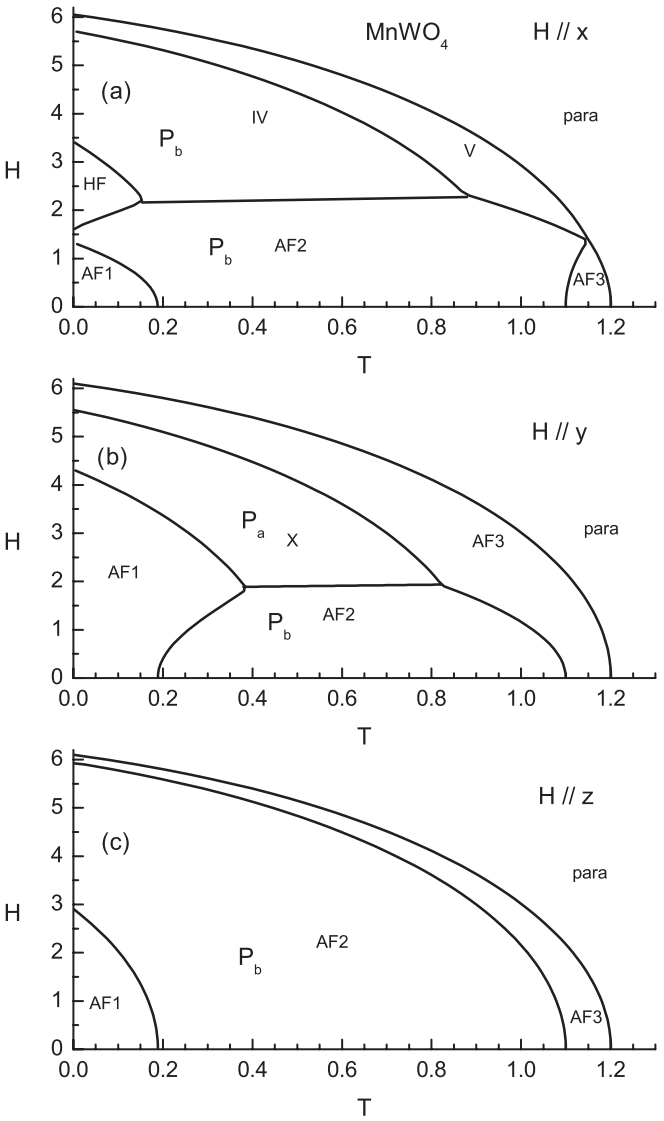

FIG. 1. Magnetic phase diagram of $MnWO_4$ for (a) H parallel to the easy axis ($\hat{x}$), (b) H parallel to the b axis ($\hat{y}$), and (c) H parallel to the hard axis ($\hat{z}$). Magnetoelectric phases are indicated by P_a and P_b.

With all parameters set, the magnetic phase of $MnWO_4$ has been determined by numerical minimization of the total free energy $F = F_s + F_E$ for different field directions, without adjusting any parameters. For an easy comparison with published experimental data on $MnWO_4$,[19] we present in Fig. 1 the magnetic phase diagrams obtained for a field applied along the easy axis ($\hat{x}$), a field parallel to the b axis ($\hat{y}$), and for a field simultaneously normal to the easy and b axis ($\hat{z}$). For clarity we also identify the different phases using the labeling sequence found in Ref. 19.

At zero field the model predictions agree with corresponding neutron scattering data.[12] At low temperatures the period-4 collinear phase (AF1) is stabilized with the moments along the easy axis ($\hat{x}$). In the intermediate temperature range a spiral order with the moments in a plane formed by the

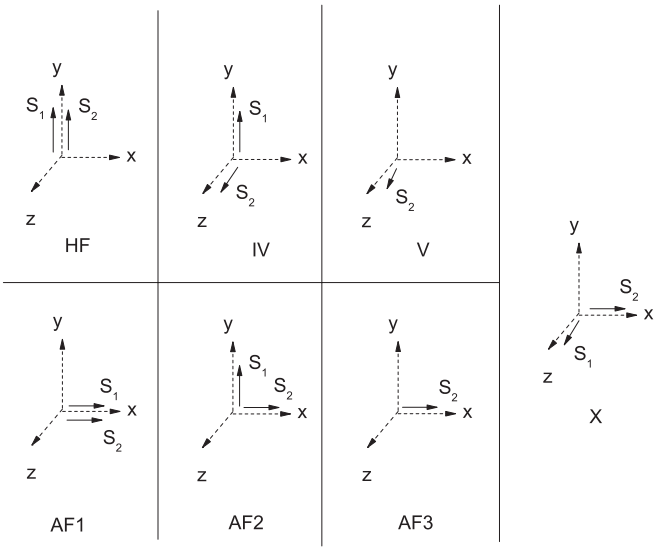

FIG. 2. Spin polarization of the magnetic states of $MnWO_4$. The canting of the spins associated with the induced magnetization are not shown here.

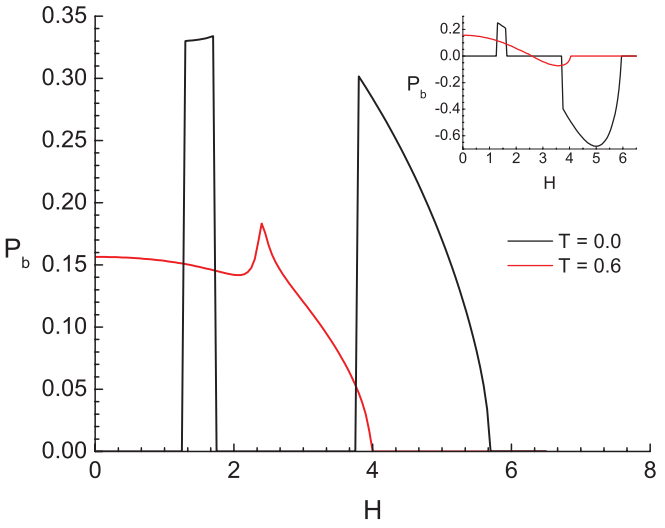

FIG. 3. (Color online) Field dependence of the induced polarization P_b calculated at $T = 0$ and $T = 0.6$ for the field along the easy-axis x. The inset show the same calculations with the higher magnetoelectric coupling term $\zeta \mathbf{P} \cdot \mathbf{P}_{\mathrm{ME}} m^2$.

b axis ($\hat{y}$) and the easy axis ($\hat{x}$) occurs (AF2). Finally, at higher temperatures a collinear sinusoidal order emerges with spins ordered only along the easy magnetization direction ($\hat{x}$). Furthermore, minimization of the free energy with respect to the polarization shows that the chiral order (AF2) induces an electric polarization pointing along the b axis, as determined experimentally.[11,21]

With the field oriented along each of the three axes (see Fig. 1), the analysis of the model reveals seven different phases, consistent with the experimental observations. In general, the qualitative agreement between the numerical predictions and the experimental data, for different field directions, is remarkable. For example, with the field applied along the b axis ($\hat{y}$), the field dependence of the boundary associated with the AF1 state emerges spontaneously. A more detailed discussion of the phase diagram associated with each field direction is presented below.

A. $H \parallel$ easy axis ($\hat{x}$)

As the field along the easy axis ($\hat{x}$) increases, numerical calculations at $T = 0$ show a first-order phase transition between the AF1 to the AF2 state. Here spins antiparallel to the field flip to the b direction, leading to the AF2 incommensurate chiral order also observed at zero field. At higher fields, moments still parallel to the field (easy axis) suddenly flip to the b axis. This first-order transformation gives rise to a new period-4 commensurate state HF with the moments pointing along the b axis. With further increase in field, the phase HF is replaced by a new chiral configuration (IV) which induces an electric polarization pointing along the b axis ($\hat{y}$). Finally, our model indicates that phase V corresponds to a sinusoidal incommensurate configuration with moments only aligned along the b axis ($\hat{y}$). Here this configuration minimizes the energy as the moments are normal to the field. The b axis is favored as it corresponds to the intermediate easy axis. A description of the magnetic phases is illustrated in Fig. 2 where the spin polarization vectors are given relative to the easy axis ($\hat{x}$), the intermediate easy axis ($\hat{y}$), and the hard axis ($\hat{z}$).

Figure 3 shows the field dependence of the polarization P_b determined at $T = 0$ and $T = 0.6$ with the magnetic field along $\hat{x}$. As AF1, HF, and phase V correspond to collinear magnetic states, the electric polarization vanishes, while the magnetic chiral states (AF2 and IV) support a polarization along the b axis. Numerical calculations performed at $T = 0.6$ also indicate that, due to the magnetoelectric coupling [Eq. (6)], magnetic moments initially parallel to the easy axis ($\hat{x}$) gradually rotate toward the hard-axis direction ($\hat{z}$) as H increases. This observation is supported by additional simulations which omitted the coupling term and in that case the moment suddenly flips from the $\hat{x}$ direction to $\hat{z}$. Thus, as shown in Fig. 3, the rotation of the chiral plane results in a maximum on the polarization P_b, which coincides with the AF2–IV phase boundary. However, note that the experimental results rather show a change in the sign of the polarity of P_b between AF2 and IV. We believed that this behavior can be attributed to higher order terms not considered in the present model. Considering the large number of possible six-order invariant terms, it would be cumbersome to carry out a detailed analysis of each contributions. Nevertheless, we present in the inset of Fig. 3 the effect of including the higher magnetoelectric coupling term $\zeta \mathbf{P} \cdot \mathbf{P}_{\mathrm{ME}} m^2$. In that case, the model does account for the change in sign of the polarity. Considering that the polarization is given by $P_b \propto S_{1b} S_{2c'} \propto \sin\gamma$ [Eq. (8)], where γ is the angle that the moments make in the ac' plane relative to the a axis, we conclude that the chiral plane must be normal to the c' axis in order to switch the polarity of the polarization P_b.

B. $H \parallel b$ axis ($\hat{y}$)

With the field applied along the b axis, a new phase X is stabilized above the chiral phase AF2 as shown in Fig. 1(b). According to our calculations, this phase results from the flip

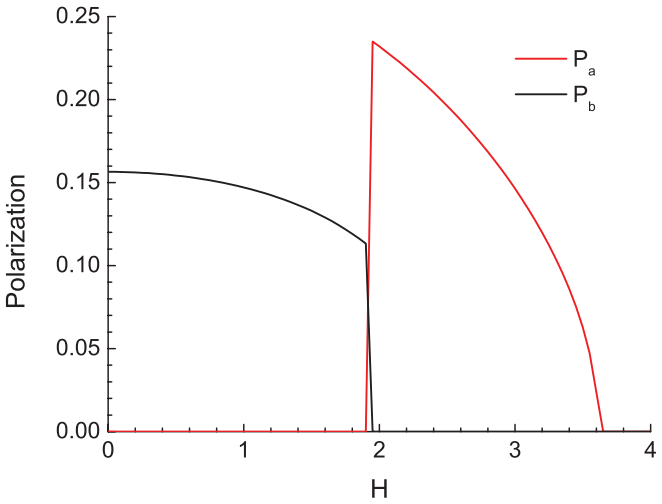

FIG. 4. (Color online) Field dependence (**H** ∥ **b**) of the induced polarization P showing the polarization flip from the b axis to the a axis at $T = 0.6$.

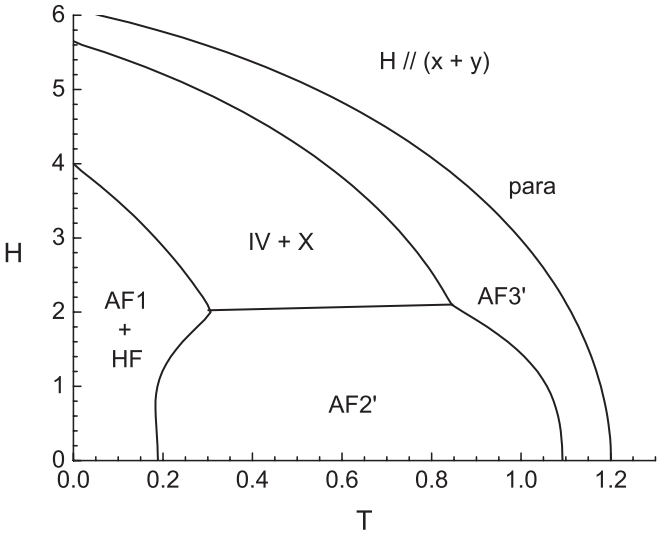

FIG. 5. Magnetic phase diagram of $MnWO_4$ for a field 45° away from the easy direction ($\hat{x}$) in the xy plane.

of **S** from b to the hard axis ($\hat{z}$). As shown in Fig. 2, the resulting phase is therefore a new chiral ordered state with the moments in the ac plane (equivalent to the xz plane). Thus, the polarization switches to the a direction [see Eq. (8)]. This is illustrated in Fig. 4 which shows the numerical predictions for both polarizations for a field scan crossing the AF2–X phase boundary ($T = 0.6$). These results agree well with experimental observations.[10,19] Naturally, as phases AF3 and AF1 correspond to collinear orders no polarization is detected.

C. H ∥ hard axis ($\hat{z}$)

For a field applied along the hard axis, no new magnetic order is obtained, as shown in Fig. 1(c). This is to be expected as all moments lay in the xy plane at zero field. The application of a field along z only results in the canting of the moments out of that plane, inducing a magnetization along the field direction.

D. H ∥ ($\hat{x}$ + $\hat{y}$)

To complete our comparison between model and experimental results for the magnetic properties of $MnWO_4$, we present in Fig. 5 the magnetic phase diagram for a field 45° away from the easy direction ($\hat{x}$) in the xy plane.[19] At low temperatures we find that the magnetic order corresponds to a commensurate spin configuration (↑↑↓↓) with the moments gradually rotating from the easy axis toward the field direction as the field is increased. Considering that the moments remain in the xy plane, this state can be described as a superposition of the collinear phases AF1 and HF. As the moments become parallel to the field direction, we observe a first-order transition to a chiral state corresponding to the superposition of the IV and X state. These observations are supported by the calculated field dependence of the polarizations shown in Fig. 6 for $T = 0$ and 0.6. In the IV + X phase we find that the polarization has components along both a and b directions. Moreover, due to the tilt of the moments within the chiral plane, a small polarization along the a axis is obtained in the AF2′ state.

V. MAGNETIC PHASE DIAGRAM OF CuO

The proposed model is also relevant for other monoclinic ferroelectrics. This can be illustrated by applying it to examine the properties of the high temperature multiferroic compound CuO (also see Ref. 20), which shows the same sequence of magnetic ordering as in $MnWO_4$ at zero field. However, in this case the easy axis is the b axis, while the intermediate easy axis is in the ac plane.[33] Therefore, in order to properly account for the anisotropic properties of CuO, we set $A_y = -0.02$, $A_{xy} = -0.01$, and $A_x = 0.012$ with $B_u = 0.02464$, $C_x = 2.0$, $Cy = 3.0$, $C_z = 2.5$, and $\zeta = 0.027$, while the other coefficient values remain unchanged. Moreover, CuO is composed of Cu ion sheets formed by two set of chains with ferro and antiferromagnetic coupling, respectively.[9] In

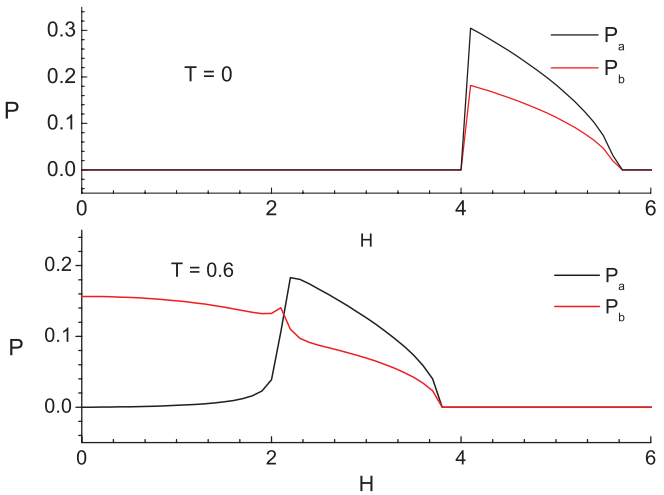

FIG. 6. (Color online) Field dependence of the induced polarization **P** for a field 45° away from the easy direction ($\hat{x}$) in the xy plane.

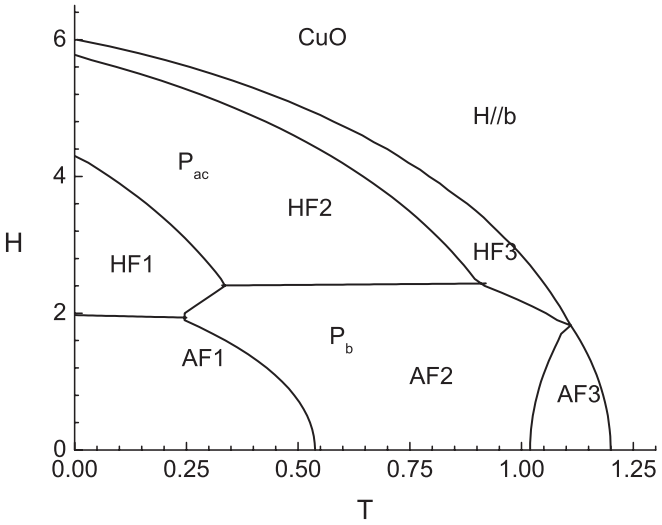

FIG. 7. Magnetic phase diagram of CuO for H parallel to the b axis. The direction of the polarization of the magnetoelectric phases are indicated by P_b and P_{ac}.

this case the magnetoelectric energy reduces to

$$\begin{aligned}\mathbf{F}_{\mathrm{ME}} = -2\alpha\{&(S_{1a}S_{2c} - S_{1c}S_{2a})P_a \\ &+ [(S_{1a} - S_{1c})S_{2b} + S_{1b}(S_{2c} - S_{2a})]P_b \\ &+ (S_{1a}S_{2c} - S_{1c}S_{2a})P_c\}. \end{aligned} \quad (9)$$

As the AF2 chiral state has $\mathbf{S}_1 = S\hat{b}$, the magnetoelectric coupling leads to a polarization along the b axis.

As the b axis is the easy axis, the magnetic phase diagram for CuO derived for a field parallel to the b axis (Fig. 7) can be compared to the one obtained for $MnWO_4$ with the field along the $\hat{x}$ direction (see Fig. 1). We notice that for $T > 0.3$ the results derived for CuO are very similar to those obtained for $MnWO_4$. We obtain the magnetic orders illustrated in Fig. 2 in terms of the easy axis ($\hat{x}$), the intermediate easy axis ($\hat{y}$), and the hard axis ($\hat{z}$). Thus the field induces phase HF1 is equivalent to HF, HF2 is IV, and AF3 is analog to V. So far, recent experimental ultrasonic velocity measurements on CuO have confirmed the existence of the phases AF1, AF2, AF3, and HF1.[20] As well, note that the polarization associated with the chiral state HF2 should be pointing in the ac plane according to Eq. (9). For a field applied along the intermediate easy axis and along the hard axis, the numerical magnetic field diagrams are similar to those presented in Fig. 1 for $H \parallel \hat{y}$ and $H \parallel \hat{z}$. Our calculations also indicate that the polarization remains along the b axis between the AF2 and X chiral state. Therefore, additional measurements at higher fields ($H >$ 16 T) are required to fully support the model's predictions for CuO.

VI. SUMMARY AND CONCLUSIONS

This work has demonstrated that a comprehensive explanation of the complex magnetic-field–temperature phase diagrams of a class of monoclinic magnetoelectric compounds can be made from an analysis of a nonlocal Landau-type free energy constructed from symmetry arguments. Experimental results in the case of $MnWO_4$ are reproduced for the field applied along each of the principal crystallographic axes as well as in one other high-symmetry direction. High-field spin states not yet examined by neutron scattering are described in detail by the model. By including a magnetoelectric coupling term, the predicted electric polarization induced by noncollinear spin configurations are described and agree with experimental results. Corresponding results for CuO with the field applied along the easy axis are also included and agree well with the observed phase diagram in that case. Our analysis of the phenomenological model leads to the prediction that for the field applied along the other axes, the phase diagrams should be similar to $MnWO_4$.

Future work will include a study of the doped compound $Mn_{1-x}Co_xWO_4$, where recent neutron diffraction results have revealed a complex phase diagram as a function of x and temperature.[27] Substitution of Mn with Co modifies the local magnetocrystalline anisotropy and can be described in our model through variations in the second-order coefficients A_{ij}. There is also evidence for a phase (AF4 + AF5) where the spin configuration is described by more than one wave vector which can be accounted for by adding a term to Eq. (3).

In summary, the results presented here, in conjunction with previous work on $CuFeO_2$, show that symmetry considerations applied to a simple mean-field model which includes the inverse DM magnetoelectric coupling term provides a powerful tool for the description of magnetic and electric polarization ordering for a wide class of magnetoelectric compounds.

ACKNOWLEDGMENTS

This work was supported by the Natural Sciences and Engineering Research Council of Canada (NSERC).

[1]T. Kimura, T. Goto, H. Shintani, K. Ishizaka, T. Arima, and Y. Tokura, Nature (London) **426**, 55 (2003).
[2]K. Wang, J.-M. Liu, and Z. Ren, Adv. Phys. **58**, 321 (2009).
[3]T. Kimura, Annu. Rev. Mater. Res. **37**, 387 (2007).
[4]Y. Tokura and S. Seki, Adv. Mater **22**, 1554 (2010).
[5]M. Fiebig, J. Phys. D: Appl. Phys. **38**, R123 (2005).
[6]T. Goto, T. Kimura, G. Lawes, A. P. Ramirez, and Y. Tokura, Phys. Rev. Lett. **92**, 257201 (2004).
[7]T. Kimura, J. C. Lashley, and A. P. Ramirez, Phys. Rev. B **73**, 220401 (2006).
[8]K. Kimura, H. Nakamura, K. Ohgushi, and T. Kimura, Phys. Rev. B **78**, 140401 (2008).
[9]T. Kimura, Y. Sekio, H. Nakamura, T. Siegrist, and A. P. Ramirez, Nat. Mater. **7**, 291 (2008).
[10]K. Taniguchi, N. Abe, T. Takenobu, Y. Iwasa, and T. Arima, Phys. Rev. Lett. **97**, 097203 (2006).
[11]A. H. Arkenbout, T. T. M. Palstra, T. Siegrist, and T. Kimura, Phys. Rev. B **74**, 184431 (2006).
[12]G. Lautenschläger, H. Weitzel, T. Vogt, R. Hock, A. Böhm, M. Bonnet, and H. Fuess, Phys. Rev. B **48**, 6087 (1993).

[13]R. Chaudhury, F. Yen, C. de la Cruz, B. Lorenz, Y. Wang, Y. Sun, and C. Chu, Physica B: Condens. Matter **403**, 1428 (2008).
[14]F. Ye, R. S. Fishman, J. A. Fernandez-Baca, A. A. Podlesnyak, G. Ehlers, H. A. Mook, Y. Wang, B. Lorenz, and C. W. Chu, Phys. Rev. B **83**, 140401 (2011).
[15]V. Felea, P. Lemmens, S. Yasin, S. Zherlitsyn, K. Y. Choi, C. T. Lin, and C. Payen, J. Phys.: Condens. Matter **23**, 216001 (2011).
[16]V. P. Sakhnenko and N. V. Ter-Oganessian, J. Phys.: Condens. Matter **22**, 226002 (2010).
[17]S. Matityahu, A. Aharony, and O. Entin-Wohlman, Phys. Rev. B **85**, 174408 (2012).
[18]I. Urcelay-Olabarria, J. M. Perez-Mato, J. L. Ribeiro, J. L. Garcia-Muñoz, E. Ressouche, V. Skumryev, and A. A. Mukhin, Phys. Rev. B **87**, 014419 (2013).
[19]H. Mitamura, T. Sakakibara, H. Nakamura, T. Kimura, and K. Kindo, J. Phys. Soc. Jpn. **81**, 054705 (2012).
[20]R. Villarreal, G. Quirion, M. L. Plumer, M. Poirier, T. Usui, and T. Kimura, Phys. Rev. Lett. **109**, 167206 (2012).
[21]H. Sagayama, K. Taniguchi, N. Abe, T.-h. Arima, M. Soda, M. Matsuura, and K. Hirota, Phys. Rev. B **77**, 220407 (2008).
[22]M. L. Plumer and A. Caillé, Phys. Rev. B **37**, 7712 (1988).
[23]M. L. Plumer, K. Hood, and A. Caillé, Phys. Rev. Lett. **60**, 45 (1988).
[24]S. G. Condran and M. L. Plumer, J. Phys,: Cond. Matter **22**, 162201 (2010).
[25]G. Quirion, X. Han, and M. L. Plumer, Phys. Rev. B **84**, 014408 (2011).
[26]M. L. Plumer, Phys. Rev. B **78**, 094402 (2008).
[27]F. Ye, S. Chi, J. A. Fernandez-Baca, H. Cao, K.-C. Liang, Y. Wang, B. Lorenz, and C. W. Chu, Phys. Rev. B **86**, 094429 (2012).
[28]M. L. Plumer, Phys. Rev. B **44**, 12376 (1991).
[29]M. B. Walker, Phys. Rev. B **22**, 1338 (1980).
[30]M. L. Plumer and M. B. Walker, J. Phys. C **15**, 7181 (1982).
[31]I. A. Sergienko and E. Dagotto, Phys. Rev. B **73**, 094434 (2006).
[32]H. Katsura, N. Nagaosa, and A. V. Balatsky, Phys. Rev. Lett. **95**, 057205 (2005).
[33]P. J. Brown, T. Chattopadhyay, J. B. Forsyth, V. Nunez, and F. Tasset, J. Phys. Condens. Matter **3**, 4281 (1991).